World Academy of Science, Engineering and Technology
International Journal of Materials and Metallurgical Engineering
Vol:18, No:10, 2024

Structural and Optical Properties of Silver Sulfide-Reduced Graphene Oxide Nanocomposite

Oyugi Ngure Robert, Tabitha A. Amollo, Kallen Mulilo Nalyanya

***Abstract*—**Nanomaterials have attracted significant attention in research because of their exemplary properties, making them suitable for diverse applications. This paper reports the successful synthesis as well as the structural and optical properties of silver sulfide-reduced graphene oxide (Ag_2S-rGO) nanocomposite. The nanocomposite was synthesized by the chemical reduction method. Scanning electron microscopy (SEM) showed that the reduced graphene oxide (rGO) sheets were intercalated within the Ag_2S nanoparticles during the chemical reduction process. The SEM images also showed that Ag_2S had the shape of nanowires. Further, SEM energy dispersive X-ray (SEM EDX) showed that Ag_2S-rGO is mainly composed of C, Ag, O, and S. X-ray diffraction analysis manifested a high crystallinity for the nanowire-shaped Ag_2S nanoparticles with a d-spacing ranging between 1.0 Å and 5.2 Å. Thermal gravimetric analysis (TGA) showed that rGO enhances the thermal stability of the nanocomposite. Ag_2S-rGO nanocomposite exhibited strong optical absorption in the UV region. The formed nanocomposite is dispersible in polar and non-polar solvents, qualifying it for solution-based device processing. Thus, the surface plasmon resonance effect associated with metallic nanoparticles, strong optical absorption, thermal stability crystallinity and hydrophilicity of the nanocomposite suits it for solar energy conversion applications.

***Keywords*—**Silver sulfide, reduced graphene oxide, nanocomposite, structural properties, optical properties.

I. Introduction

NANOCOMPOSITES are significantly gaining research interest in the twenty-first century. Unlike traditional composites, nanocomposites possess unique properties and designs [1]. Nanoparticles are tiny materials ranging between 1 and 100 nm [2]. The nanoparticles' nanoscale size and high surface area give them desirable and unique properties. For instance, silver nanoparticles have more advanced chemical, biological, and physical characteristics than their macro-scaled particles [3]. Silver nanoparticles' advanced physical and chemical properties include high thermal and electrical conductivity, enhanced chemical stability, surface-enhanced Raman Scattering, non-linear optical behavior, and improved catalytic activity [3]. Furthermore, the nanoparticles possess other properties, such as toughness, reactivity, and other characteristics that depend on their sizes [2]. This makes the nanoparticles have a wide range of applications.

Silver sulfide nanoparticles (Ag_2S NPs) has properties that largely depend on its size, making them attractive for applications in various fields including photocatalysis and biomedicine [4]. The nanoparticles of silver sulfide have also attracted optical applications within the visible region through surface plasmon resonance [4]. The Ag_2S NPs have a monoclinic crystal structure, a significant absorption coefficient [5], a narrow band gap (between 0.9 eV to 1.05 eV) [6], good chemical stability, and photoconductivity [4]. The uniqueness of these properties also makes the nanomaterials applicable in various areas, including sensors, food packaging, drug delivery, conductive paints, rechargeable batteries, and active electronic devices [7]. Nanoparticles are also applicable in energy conversion, where they offer surface plasmon resonances which enhance the trapping of light and allow for the tuning of resonant wavelengths [8]. Silver nanowire is one of the nanoparticles that are effective in trapping light through Localized Surface Plasmon Resonance (LSPR) [5]. In a nanocomposite, two nanomaterials are brought together resulting in enhanced properties since they combine the different materials' properties.

Graphene is a monolayer 2D nanomaterial of sp^2-hybridized carbon atoms densely packed in a honeycomb lattice structure [9]. Graphene has desirable mechanical properties, i.e., a break strength of 42 Nm^{-1} [10], an intrinsic tensile strength of 130.5 GPa, and 1.0 TPa Young's modulus [11] and high charge carrier mobility [10]. Graphene oxide (GO) is an oxidized form of graphene having oxygen functional groups that decorate the basal planes of C [12]. GO has hydroxylic and epoxy oxygen functional groups on the basal planes and the carboxylic group on the edges [13]. GO also has hydrophilic properties, making it possible to disperse in water or solvents, as opposed to graphene, which is hydrophobic. It is also possible to tune the sizes of GO variedly between a few nm and μm, giving them an advantage in wide applications. GO in its reduced form has been applied in electronic devices, biomedical applications, energy storage, supercapacitors, biosensors, catalysts, water purification, and membranes [14]. Removing oxygen functional groups from GO during the reduction process restores the sp^2-conjugated graphene network, thereby improving electron transport [15]. The reduced GO has sheets like that of graphene and restores the p-conjugated structure [16]. The GO's electrical conductivity is inferior to that of graphene because of the oxygen functional groups. In its reduced form, the rGO becomes electrically conductive and has defect sites [16].

In this study, Ag_2S-rGO nanocomposite was synthesized using chemical reduction method. This method can be carried

Oyugi N. Robert and Kallen M. Nalyanya are with Egerton University, Faculty of Science, Department of Physics, P.O Box 536-20115, Egerton, Nakuru, Kenya.

Tabitha A. Amollo is with Egerton University, Faculty of Science, Department of Physics, P.O Box 536-20115, Egerton, Nakuru, Kenya and with University of Pretoria, Future Africa, Private Bag 20, Hatfield, England (corresponding author, e-mail: tamollo@egerton.ac.ke).

out at room temperature [17]. The advantages of the chemical reduction method are that it can achieve mass production of the nanocomposite [17], it is cost-effective, has a good production rate [18], and allows for the control of the chemical composition [19]. Obtaining homogeneous and stable solutions in synthesizing nanocomposites based on graphene is necessary [20]. Thus, GO was appropriate for synthesizing the nanocomposite since it has oxygen functional groups below and above the basal planes, providing nucleation sites for doping heteroatoms [21]. It is envisaged that the synergistic effect of LSPR of the NPs and the outstanding properties of graphene would suit the nanocomposite for optoelectronic applications such as in solar cells.

II. Experimental

A. Materials

The following materials were purchased from Kobian, Kenya: Silver Nitrate ($AgNO_3$), Polyvinylpyrrolidone (PVP), graphite powder, sodium nitrate, concentrated sulphuric acid, potassium permanganate, hydrogen peroxide (3%), and sodium sulfide. The purity of these materials was 99.95%, 99%, 99.99%, > 99.0%, 99.999%, > 99.0%, 30%, and 99.999%, respectively. Absolute ethanol was also purchased from Kobian, Kenya.

B. Synthesis

1. Synthesis of Graphene Oxide

Graphene Oxide was synthesized using the modified Hummers method [22]. The process started by mixing 1 g of sodium nitrate, 1 g of graphite powder, and 50 ml of concentrated sulphuric acid and stirring for 30 minutes at 0 °C. 6 g of potassium permanganate was then added to the mixture. The process was followed with further stirring for 3 hours at 35 °C. 200 ml of hydrogen peroxide (3%) was added, stirring the solution for 30 minutes [13]. The obtained solution was washed to a neutral pH with double distilled water. GO films were obtained by drying the solution at 50 °C in a vacuum oven.

2. Synthesis of Silver Sulphide Nanoparticles and Ag_2S-rGO Nanocomposite

The synthesis of Ag_2S nanoparticles followed the protocol of [5]. It started with the preparation of various precursor solutions. 1.698 g (0.1M) of silver nitrate hexahydrate ($Na_2S.6H_2O$), 3.0 g of polyvinyl pyrrolidone (PVP), and 0.4 g (0.1 M) of sodium sulfide were separately dissolved in 50 mL of double distilled water. The PVP and sodium sulfide solutions were mixed dropwise into silver nitrate solution under stirring with a magnetic stirrer. The solution mixture was then stirred continuously for 3 hours. The precipitate was then centrifuged for 5 minutes at 4500 revolutions per minute. A successive washing with ethanol and double distilled water followed. The residue was then dried in an oven at 80 °C for 3 hours to obtain Ag_2S nanoparticles. For the synthesis of Ag_2S-rGO nanocomposite, GO at varied concentrations of 10 mg, 20 mg, 50 mg, 100 mg, and 150 mg in 10 ml, 20 ml, 50 ml, 100 ml, and 150 ml of double-distilled water, respectively, was injected into the mixture of sodium sulfide, silver nitrate, and PVP. This was further stirred for 1 hr. The solution mixture obtained was centrifuged and washed with ethanol and double distilled water. The final residue was dried for 8 hours in a vacuum oven at 80 °C.

C. Characterization

A field emission SEM (SEM: Phenom Pro by Thermofisher) was used to determine the morphological properties of the materials. Electron Dispersive X-ray Spectroscopy (EDX) detector attached to SEM was used for elemental analysis. The structural analysis was done using XRD (MiniFlex 300/600) with Cu Kα radiation (λ = 1.5418740 Å). Powder XRD analysis for the determination of the crystallinity and the structure of the Ag_2S-rGO nanocomposite was done with a scanning range of 2θ from 10° to 90° and a scanning speed of 10 °/min. The essence of the XRD is that it helps determine the material's bulk structure. Fourier transform infrared (FTIR) spectroscopy was used to determine the oxygen functional groups in Ag_2S-rGO nanocomposite using Perkin Elmer spectrum 100 FTIR. A UV-Vis spectrophotometer (UV-1900i by Shimadzu) was used to characterize the optical absorption of the nanomaterials dispersed in ethanol at various wavelengths.

III. Results and Discussion

A. Morphological Properties

Analysis of the morphological properties of the synthesized Ag_2S-rGO nanocomposite was done using SEM, and the obtained images are shown in Figs. 1 and 2. Fig. 1 shows Ag_2S of nanowire shape. The nanowires of Ag_2S possesses unique optoelectronic, electrical, and mechanical properties [23]. Fig. 2 indicates a tightly packed structure of folded rGO. The observed structure resonates with [24] demonstration that rGO possesses a tightly packed interlocking sheet structure. The importance of this structure is that rGO becomes uniformly distributed onto the surface of the Ag_2S, hence obtaining homogeneity in the synthesized nanocomposite. Moreover, research indicates that when GO gets chemically converted to graphene, defects and vacancies are produced in the carbon structure [25]. Consequently, it is possible that crystals of Ag_2S grow around these defects and vacancies as they are inclined to interact with the introduced graphene sheets during the formation of the nanocomposite.

B. SEM-EDX Analysis

The nanocomposite was subjected to SEM-EDX elemental analysis, and the obtained spectrum is shown in Fig. 3. The essence of EDX analysis is that it reveals the elements present in the samples, as observed in Fig. 3; the elements in the Ag_2S-rGO nanocomposite include C, Ag, O, and S. The C and O peaks in the EDX spectrum indicated the presence of rGO in the nanocomposite. Additionally, only one O peak, with low intensity, was observed, implying the successful reduction of the GO. The distribution of the elemental peaks in the EDX spectrum also suggests that the elements are distributed throughout the rGO matrix and are not confined to limited space [26]. Such a distribution of the elements confirms the

uniformity of the nanocomposite. The purity of the nanocomposite is approved by the non-presence of extra signals in the EDX spectrum.

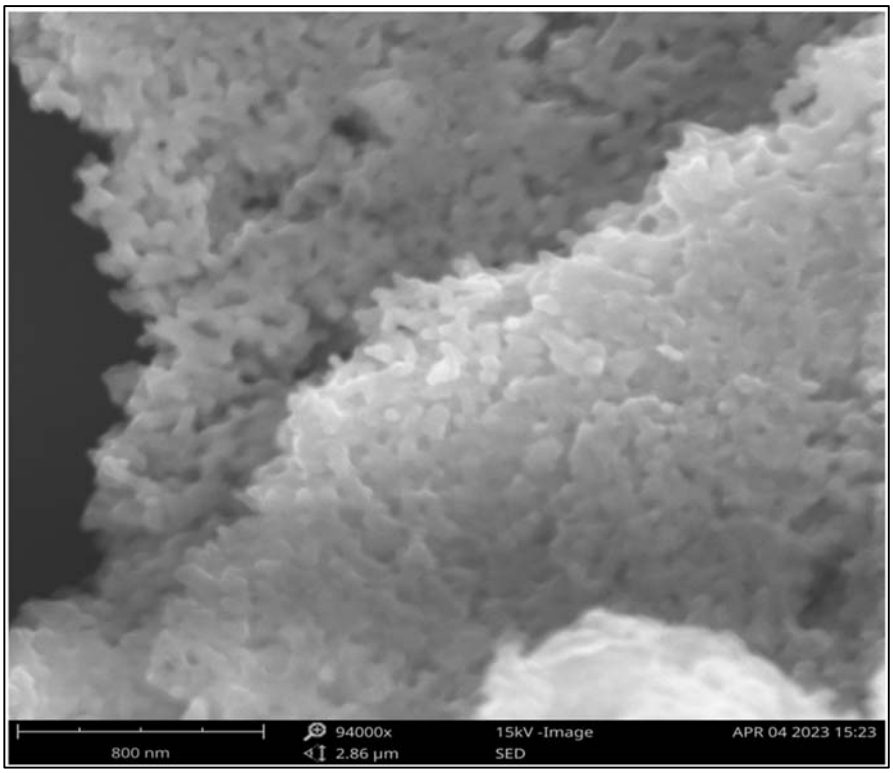

Fig. 1 SEM image of Ag_2S-rGO with GO concentration of 150 mg

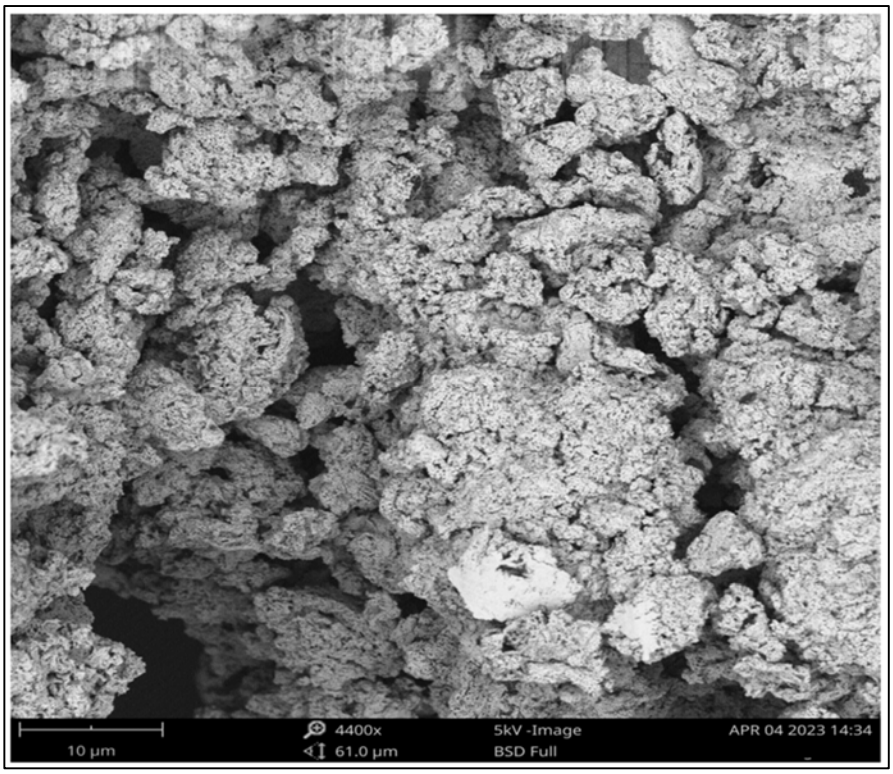

Fig. 2 SEM Images of Ag_2S-rGO with GO concentration of 10 mg

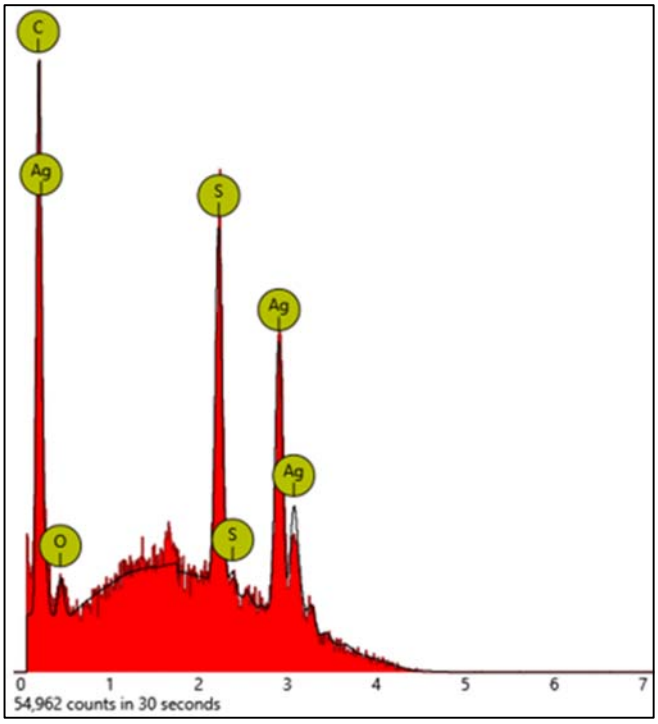

Fig. 3 SEM-EDX Analysis of $Ag_2S - rGO$ nanocomposite

C. Structural Properties

The XRD patterns for the Ag_2S and Ag_2S-rGO are shown in Fig. 4. The major diffraction peaks of Ag_2S were observed at 2θ values of 17.2°, 22.4°, 24.9°, 25.9°, 26.3, 28.9°, 31.5°, 33.6°, 34.38°, 34.7°, 36.8°, 37.7°, 40.7°, 43.4°, 46.2°, 47.8°, 48.7°, 53.2°, 58.3°, and 63.7°. According to the Joint Committee on Powder Diffraction Standards (JCPDS) card 96-900-0254, the diffraction peaks shown in Fig. 4 (a) correspond to the (011), (10-1), (110), (11-1), (022), (021), (111), (120), (120), (-121), (112), (013), (-113), (122), (210), (20-2), (113), (220), (221), and (-142) lattice planes of Ag_2S, respectively [27]. These diffraction peaks indicate a monoclinic acanthite phase of Ag_2S. The d-spacing of the diffraction lines ranged between 1.0 Å and 5.2 Å, indicating that the Ag_2S is a nanoparticle.

The diffraction peaks observed in Fig. 4 (b) in the nanocomposite at 2θ values of 26.3°, 44.3°, 54.2°, 83.2°, and 85.0° are additional to the ones for Ag_2S in Fig. 4 (a) and correspond to the (002), (101), (400), (112), and (006) crystalline planes of rGO, respectively (JCPDS-card 01-075-1621). The most substantial peak observed at 2θ = 26.3° corresponding to the miller index of (002) of carbon with a d-spacing of 3.395 Å coincides with the (022) lattice plane of Ag_2S nanoparticle, further demonstrating the uniformity of the nanocomposite formed [28]. The lack of diffraction peaks below 12.0°, which is the known diffraction peak for GO, indicates the successful reduction of GO during the chemical reduction process [28], [29].

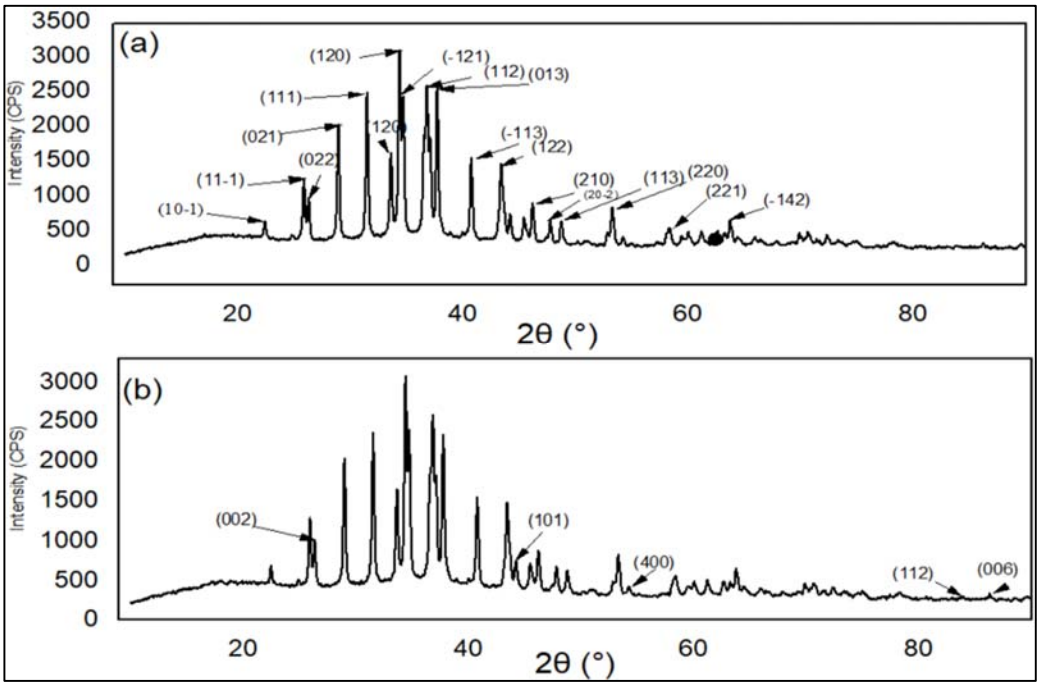

Fig. 4 XRD patterns for (a) Ag_2S and (b) Ag_2S-rGO nanocomposite

D. Thermal Stability

The TGA was used to investigate the thermal stability of Ag_2S nanoparticles and Ag_2S-rGO nanocomposite and the results are shown in Fig. 5. The nanoparticles and the nanocomposite were heated from room temperature to 1000 °C in a nitrogen gas atmosphere. The heating rate was set at 10 °C per minute. The TGA of Ag_2S nanoparticles demonstrated a three-phase decomposition behavior, as seen in Fig. 5 (a). The

weight loss was observed in the temperature ranges of 300 °C to 480 °C, 520 °C to 700 °C, and 760 °C to 850 °C.

The slight mass loss of Ag_2S from 300 °C to 480 °C is attributed to the desorption of the water molecules from the surface of the nanoparticles [30]. When Ag_2S nanoparticles get heated above the temperature of 175 °C; there is a transition of acanthite to the argentite phases of the Ag_2S [31]. The region between 227 °C and 527 °C exhibits argentite of Ag_2S [31]. This is the high weight loss observed from 300 °C to 480 °C. Silver sulphide also exhibits other beta and gamma phases at higher temperatures. For instance, above 160 °C, Ag_2S exhibits β argentite phase while above 587 °C, it contains $\gamma - Ag_2S$ phase [31]. After the transformation of Ag_2S from β-Ag_2S to γ-Ag_2S, at temperatures between 627 °C and 697 °C, the thermal expansion coefficient significantly grows [31]. It is inferred that this increased coefficient of thermal expansion is responsible for the steep weight loss from 520 °C to 700 °C. The last weight loss between 760 °C and 850 °C is associated with the decomposition of the nanoparticles [30].

The first observable weight loss of Ag2S-rGO nanocomposite from the TGA occurred from below 100 °C to 210 °C (Fig. 5 (b)). This weight loss is attributed to decomposition of the oxygenated functional groups in the nanocomposite [28]. It is expected that the graphitic composition of the nanocomposite is all decomposed at 600 °C [28]. Thus, the remaining residue is of Ag_2S, which continues to decompose until a temperature of 981 °C. It is also observable that the addition of rGO to the Ag_2S slowed the rate of decomposition between 520 °C and 850 °C; hence, rGO enhances the thermal stability of Ag_2S in the nanocomposite.

The derivative thermograms (DTG) of Ag_2S is shown in Fig. 5 (c). Fig. 5 (c) shows three significant peaks at 180 °C, 580 °C, and at 733 °C. These peaks correspond to the Ag_2S phase transitions [30]. Specifically, the monoclinic acanthite of Ag_2S shows stability up to 176 °C, after which the body-centered cubic argentite becomes stable between 176 °C and 622 °C, after which there is a face-centered cubic polymorph [30]. This explains the irregular pattern in weight loss of Ag_2S at 713 °C, in which there is an increase in weight, after which there is a fall from 766 °C as seen in Fig. 5 (a).

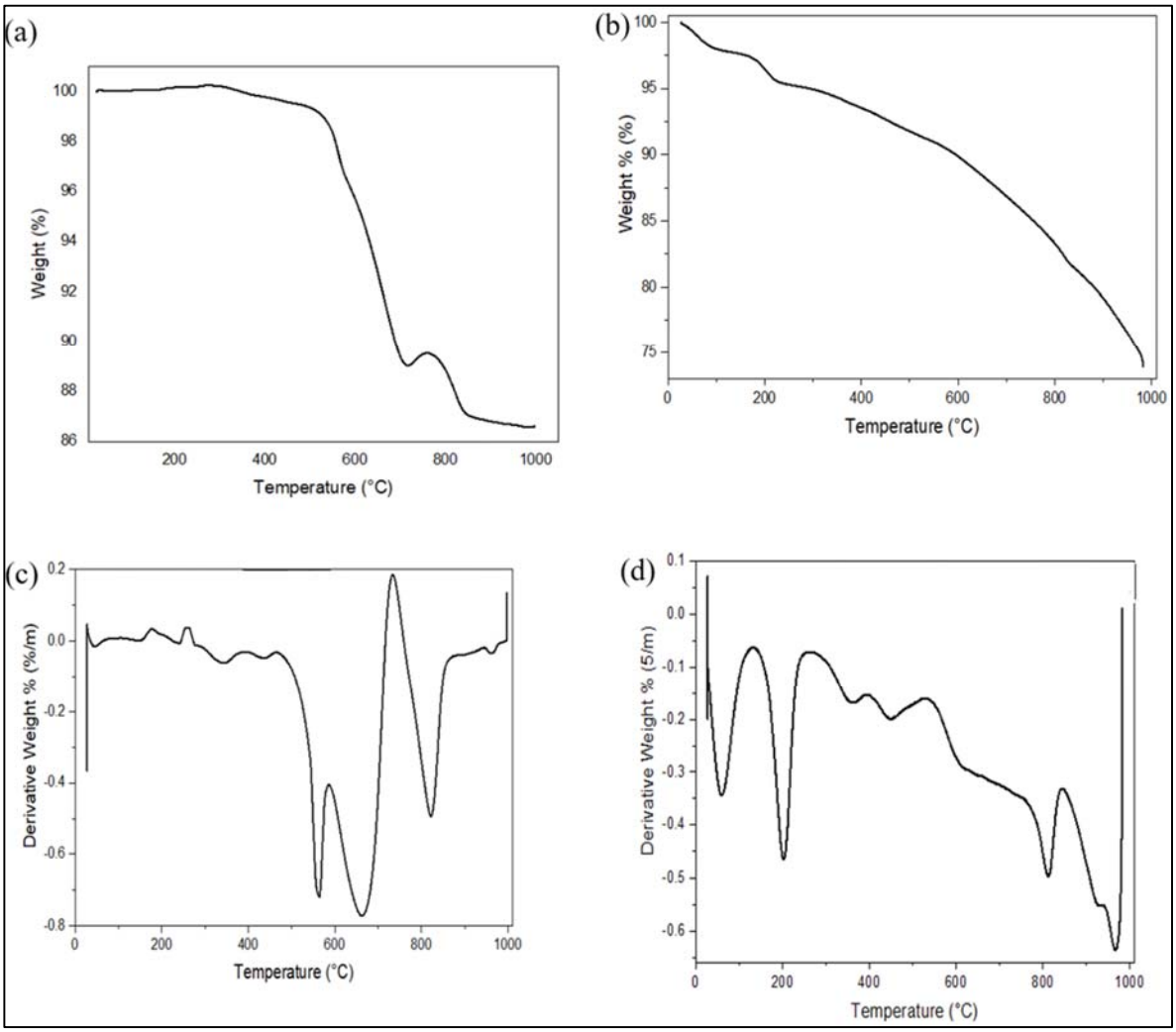

Fig. 5 TGA thermograms of (a) Ag_2S and (b) Ag2S-rGO; and derivative thermogram of (c) Ag_2S and (d) Ag2S-rGO

As shown in Fig. 5 (d), the DTA of Ag2S-rGO shows peaks at 133 °C, 260 °C, 530 °C, and 845 °C. These peaks demonstrate the phase shifts of the nanocomposite. The peak at 845 °C indicate the combustion of graphite [32]. The peak at 260 °C can be associated with removing oxygen-containing groups from the nanocomposite [33]. The endothermal peak observed at 133 °C indicate the decomposition of water molecules from the surface of the nanocomposite [34]. Since there is no other DTA peak characteristic to another element other than the main components of Ag2S-rGO, the nanocomposite can be considered to be pure.

E. Optical Absorption

The Ag2S-rGO nanocomposite was formed at different concentrations of rGO. Fig. 6 shows the UV-Vis spectra of Ag_2S and Ag2S-rGO nanocomposite. Both the Ag_2S and Ag2S-rGO nanocomposites show the highest absorption peak at 202 nm. The absorption peak at 202 nm for Ag_2S can be attributed to the surface plasmon resonance of the nanowire shape of the nanoparticle [4]. Silver nanowire effectively traps light through LSPR [5]. This can be confirmed by the observed nanowire shape of Ag_2S in the SEM image in Fig. 1. As observed in Fig. 6 (b), the peak at 202 nm is a superimposition of the absorbance of Ag2S and rGO. For, rGO the peak is characteristic of π-π* transitions of the C-C aromatic bonds [35]-[37].

Research shows that the absorbance of Ag_2S increases with an increase in wavelength from the ultraviolet to the visible region [38]. This explains why the UV-Vis spectrum of Ag_2S shows a slight increase in absorbance from 202 nm. Fig. 6 (b) shows a slight increase in the absorbance of the nanocomposite from 250 nm. Such a change in the absorbance of Ag_2S with rGO indicates increased surface plasmon resonance excitation in the visible region [39].

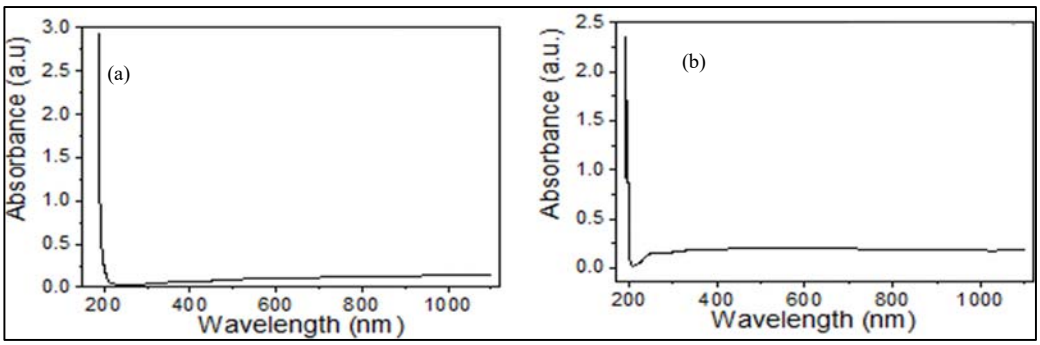

Fig. 6 Optical absorption of (a) Ag_2S and (b) Ag2S-rGO

F. Surface Chemistry

The FT-IR was conducted to determine the functional groups of the Ag2S-rGO nanocomposite. Fig. 7 (a) shows the FT-IR spectrum of Ag_2S nanoparticles, while Fig. 7 (b) shows the spectrum for Ag2S-rGO nanocomposite. For Ag_2S nanoparticles, the major bands were observed at 735 cm^{-1}, 1048 cm^{-1}, 1285 cm^{-1}, 1438 cm^{-1}, 1640 cm^{-1}, 2090 cm^{-1}, 2330 cm^{-1}, 2660 cm^{-1}, 2920 cm^{-1}, and 3840 cm^{-1}. The major peaks for Ag2S-rGO spectrum were observed at 630 cm^{-1}, 1055 cm^{-1}, 1290 cm^{-1}, 1320 cm^{-1}, 1420 cm^{-1}, 1640 cm^{-1}, 1995 cm^{-1}, 2100 cm^{-1}, 2340 cm^{-1}, 2680 cm^{-1}, 2855 cm^{-1}, 2920 cm^{-1}, 3747 cm^{-1}, and 3830 cm^{-1}.

The band at 3747 cm^{-1} for the nanocomposite indicates the presence of hydroxyl (OH) groups due to the addition of the rGO to the Ag_2S nanoparticles [40], [41]. The band at 630 cm^{-1} in Fig. 7 (b) can be associated with the C-O-C and C-O bending vibrations, [40]. A common band appears at 1640 cm^{-1} for both Ag_2S and Ag2S-rGO. The peak is resonant to the stretching and bending of OH groups in water molecules [40], [42]. It is further observable that the band at 630 cm^{-1} emerges in the Ag2S-rGO nanocomposite nanoparticles. This occurrence can be explained by the chelation of blank orbits in Ag_2S, which are deficient in electrons to the atoms in O-H that are rich in O and the sp^2-conjugated bonds on the rGO surface [43]. The IR spectrum indicates a strong interaction between the Ag_2S and the matrix of rGO confirming the immobility of Ag_2S on the GO matrix's surface.

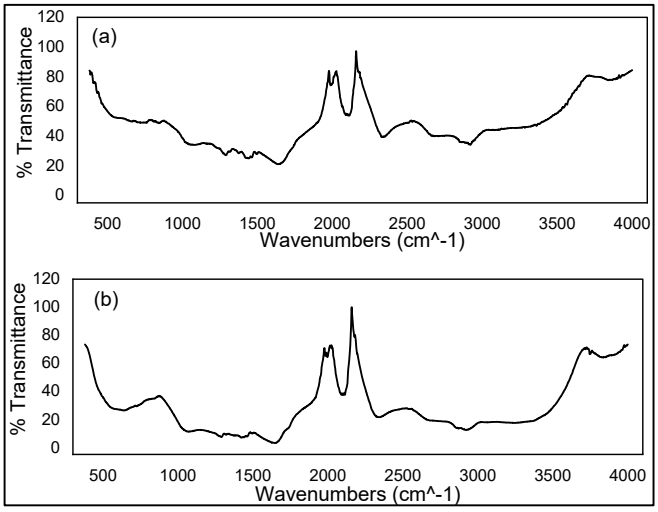

Fig. 7 IR Spectrum of (a) Ag_2S and (b) Ag2S-rGO

IV. Conclusion

Ag2S-rGO with high crystallinity was successfully synthesized using chemical reduction method. SEM image of the nanocomposite showed that rGO sheets were intercalated in

Ag_2S nanoparticles during synthesis. The SEM analysis also showed that Ag_2S had the shape of nanowires. The TGA analysis of the Ag_2S-rGO nanocomposite indicated a significant weight loss at 157 °C to 211 °C, explaining the decomposition of the oxygenated functional groups. The TGA further showed that rGO enhances the thermal stability of Ag_2S. The DTA analysis of the nanocomposite showed endothermic peaks at 133 °C, 260 °C, 530 °C, and 845 °C demonstrating the phase shifts of the nanocomposite with a DTA peak at 845 °C showing the combustion of graphite. The lack of DTA and EDX peaks for other elements other than those in the Ag_2S-rGO showed the purity of the nanocomposite.

The d-spacing for the diffraction lines in XRD ranged between 1.0 Å and 5.2 Å, indicating that the composite formed was in nanoscale. The presence of rGO in the nanocomposite was confirmed by a strong XRD peak at 2θ = 26.3°, corresponding to the miller index (002) of carbon. The nanocomposite exhibited strong optical absorbance in the UV region. FT-IR spectrum of the nanocomposite confirmed a strong interaction between Ag_2S and the matrix of rGO. The nanocomposite is easily dispersed in polar and non-polar solvents. The nanocomposite is suitable for various applications including solar energy conversion given its thermal stability, optical absorption, LSPR effect and crystallinity.

Conflict of Interest

The authors declare that no conflict of interest exists regarding this research article's submission and publication.

Funding

This research was funded by grants from the Carnegie Corporation of New York and The World Academy of Sciences (TWAS) (grant no. 20-187 RG/PHYS/AF/AC_I – FR3240314148). The statements made and views expressed are solely the author's responsibility.

Acknowledgment

The authors acknowledge BESSY II at Helmholtz-Zentrum Berlin (HZB), Germany, for assisting with SEM measurements.

References

[1] A. U. Agobi, A. J. Ekpunobi, A. I. Ikeuba, and H. Louis, "The effects of graphene oxide load on the optical, structural and electrical properties of ternary nanocomposites (Polyvinyl alcohol/copper/graphene oxide) for electronic and photovoltaic application," *Results Opt.*, vol. 8, no. 2, pp. 1–9, 2022, doi: 10.1016/j.rio.2022.100261.

[2] K. Ibrahim, K. Saeed, and I. Khan, "Nanoparticles: Properties, applications and toxicities," *Arab. J. Chem.*, vol. 12, no. 7, pp. 908–931, Nov. 2019, doi: 10.1016/j.arabjc.2017.05.011.

[3] Q. H. Tran, V. Q. Nguyen, and A.-T. Le, "Silver nanoparticles: synthesis, properties, toxicology, applications and perspectives," *Adv. Nat. Sci. Nanosci. Nanotechnol.*, vol. 4, no. 3, pp. 1–21, May 2013, doi: 10.1088/2043-6262/4/3/033001.

[4] Y. Delgado, C. E. Martinez, M. Cortez, N. S. Flores, and M. Flores, "Optical properties of silver, silver sulfide and silver selenide nanoparticles and antibacterial applications," *Mater. Res. Bull.*, vol. 99, pp. 385–392, Mar. 2018, doi: 10.1016/j.materresbull.2017.11.015.

[5] M. S. G. Hamed, M. A. Adedeji, Y. Zhang, and G. T. Mola, "Silver sulphide nano-particles enhanced photo-current in polymer solar cells," *Appl. Phys. A Mater. Sci. Process.*, vol. 126, no. 3, pp. 1–207, Mar. 2020, doi: 10.1007/s00339-020-3389-8.

[6] P. Kumari, P. Chandran, and S. S. Khan, "Synthesis and characterization of silver sulfide nanoparticles for photocatalytic and antimicrobial applications," *J. Photochem. Photobiol. B Biol.*, vol. 141, pp. 235–240, Dec. 2014, doi: 10.1016/j.jphotobiol.2014.09.010.

[7] V. S. Shanthala, S. N. Shobha Devi, and M. V. Murugendrappa, "Synthesis, characterization and DC conductivity studies of polypyrrole/copper zinc iron oxide nanocomposites," *J. Asian Ceram. Soc.*, vol. 5, no. 3, pp. 227–234, Sep. 2017, doi: 10.1016/j.jascer.2017.02.005.

[8] R. Ohib, S. Y. Arnob, M. S. Ali, R. H. Sagor, and M. R. Amin, "Metal nanoparticle enhanced light absorption in GaAs thin-film solar cell," in *2016 IEEE Asia-Pacific Conference on Applied Electromagnetics, APACE 2016*, 2016, pp. 89–93. doi: 10.1109/APACE.2016.7916482.

[9] T. A. Amollo, G. T. Mola, and V. O. Nyamori, "Organic solar cells: Materials and prospects of graphene for active and interfacial layers," *Crit. Rev. Solid State Mater. Sci.*, vol. 45, no. 4, pp. 261–288, 2020, doi: 10.1080/10408436.2019.1632791.

[10] A. T. Smith, A. M. LaChance, S. Zeng, B. Liu, and L. Sun, "Synthesis, properties, and applications of graphene oxide/reduced graphene oxide and their nanocomposites," *Nano Mater. Sci.*, vol. 1, no. 1, pp. 31–47, Mar. 2019, doi: 10.1016/j.nanoms.2019.02.004.

[11] P. Zhang *et al.*, "Fracture toughness of graphene," *Nat. Commun.*, vol. 5, pp. 1–7, 2014, doi: 10.1038/ncomms4782.

[12] F. Perrozzi, S. Prezioso, and L. Ottaviano, "Graphene oxide: from fundamentals to applications," *J. Phys. Condens. Matter*, vol. 27, no. 1, pp. 1–22, Jan. 2015, doi: 10.1088/0953-8984/27/1/013002.

[13] T. A. Amollo, G. T. Mola, and V. O. Nyamori, "High-performance organic solar cells utilizing graphene oxide in the active and hole transport layers," *Sol. Energy*, vol. 171, no. 5, pp. 83–91, 2018, doi: 10.1016/j.solener.2018.06.068.

[14] A. Jiříčková, O. Jankovský, Z. Sofer, and D. Sedmidubský, "Synthesis and Applications of Graphene Oxide," *Materials (Basel).*, vol. 15, no. 3, pp. 1–21, Jan. 2022, doi: 10.3390/ma15030920.

[15] T. A. Amollo, G. T. Mola, and V. O. Nyamori, "Polymer solar cells with reduced graphene oxide–germanium quantum dots nanocomposite in the hole transport layer," *J. Mater. Sci. Mater. Electron.*, vol. 29, no. 9, pp. 7820–7831, May 2018, doi: 10.1007/s10854-018-8781-1.

[16] N. Sharma *et al.*, "Synthesis and Characterization of Graphene Oxide (GO) and Reduced Graphene Oxide (rGO) for Gas Sensing Application," *Macromol. Symp.*, vol. 376, no. 1, pp. 1–5, Dec. 2017, doi: 10.1002/masy.201700006.

[17] R. Yousefi and M. Cheraghizade, "Semiconductor/Graphene Nanocomposites: Synthesis, Characterization, and Applications," in *Applications of Nanomaterials*, Elsevier, 2018, pp. 23–43. doi: 10.1016/B978-0-08-101971-9.00002-8.

[18] H.-R. Rahimi and M. Doostmohammadi, "Nanoparticle Synthesis, Applications, and Toxicity," in *Applications of Nanobiotechnology*, IntechOpen, 2020, pp. 1–16. doi: 10.5772/intechopen.87973.

[19] M. A. Virji and A. B. Stefaniak, "A Review of Engineered Nanomaterial Manufacturing Processes and Associated Exposures," in *Comprehensive Materials Processing*, Elsevier, 2014, pp. 103–125. doi: 10.1016/B978-0-08-096532-1.00811-6.

[20] Z. Song *et al.*, "Polymer−Graphene Nanocomposites as Ultrafast-Charge and -Discharge Cathodes for Rechargeable Lithium Batteries," *Nano Lett.*, pp. 2205–2211, 2012.

[21] D. Lv *et al.*, "GeO x /Reduced Graphene Oxide Composite as an Anode for Li-Ion Batteries: Enhanced Capacity via Reversible Utilization of Li 2 O along with Improved Rate Performance," *Adv. Funct. Mater.*, vol. 24, no. 8, pp. 1059–1066, Feb. 2014, doi: 10.1002/adfm.201301882.

[22] W. S. Hummers and R. Offeman, "Preparation of graphitic oxide," *J. Am. Chem. Soc.*, vol. 80, no. 6, pp. 1339–1339, 1958.

[23] S. I. Sadovnikov and A. I. Gusev, "Recent progress in nanostructured silver sulfide: from synthesis and nonstoichiometry to properties," *J. Mater. Chem. A*, vol. 5, no. 34, pp. 17676–17704, 2017, doi: 10.1039/C7TA04949H.

[24] O. C. Compton and S. T. Nguyen, "Graphene Oxide, Highly Reduced Graphene Oxide, and Graphene: Versatile Building Blocks for Carbon-Based Materials," *Small*, vol. 6, no. 6, pp. 711–723, Mar. 2010, doi: 10.1002/smll.200901934.

[25] S. Pan, X. Liu, and X. Wang, "Preparation of Ag2S-Graphene nanocomposite from a single source precursor and its surface-enhanced Raman scattering and photoluminescent activity," *Mater. Charact.*, vol. 62, no. 11, pp. 1094–1101, 2011, doi: 10.1016/j.matchar.2011.08.004.

[26] H. Naeem *et al.*, "Reduced Graphene Oxide-Zinc Sulfide Nanocomposite

Decorated with Silver Nanoparticles for Wastewater Treatment by Adsorption, Photocatalysis and Antimicrobial Action," *Molecules*, vol. 28, no. 3, pp. 1–19, Jan. 2023, doi: 10.3390/molecules28030926.

[27] Wiegers, "The crystal structure of the low-temperature form of silver selenide," *Am. Mineral.*, vol. 56, pp. 1882–1888, 1971.

[28] A. C. M. de Moraes, B. Araujo Lima, A. Fonseca de Faria, M. Brocchi, and O. Luiz Alves, "Graphene oxide-silver nanocomposite as a promising biocidal agent against methicillin-resistant Staphylococcus aureus," *Int. J. Nanomedicine*, pp. 6847–6861, Nov. 2015, doi: 10.2147/IJN.S90660.

[29] S. Baskar, T. Lavanya, K. Subramani, and K. Satheesh, "Synthesis and characterization of reduced graphene oxide/Ag2S nanocomposites by co-precipitation method using thiourea as sulfur source and reducing agent," *Int. J. ChemTech Res.*, vol. 9, no. 5, pp. 395–401, 2016.

[30] G. A. Martínez, M. G. Sánchez-Loredo, H. J. Dorantes, J. R. Martínez, G. Ortega, and F. Ruiz, "Characterization of silver sulfide nanoparticles synthesized by a simple precipitation method," *Mater. Lett.*, vol. 59, no. 4, pp. 529–534, Feb. 2005, doi: 10.1016/j.matlet.2004.10.043.

[31] S. I. Sadovnikov and A. I. Gusev, "Thermal expansion, heat capacity and phase transformations in nanocrystalline and coarse-crystalline silver sulfide at 290–970 K," *J. Therm. Anal. Calorim.*, vol. 131, no. 2, pp. 1155–1164, Feb. 2018, doi: 10.1007/s10973-017-6691-8.

[32] F. Farivar, P. Lay Yap, R. U. Karunagaran, and D. Losic, "Thermogravimetric Analysis (TGA) of Graphene Materials: Effect of Particle Size of Graphene, Graphene Oxide and Graphite on Thermal Parameters," *J. Carnon Res.*, vol. 7, no. 2, pp. 1–12, Apr. 2021, doi: 10.3390/c7020041.

[33] X.-Z. Tang *et al.*, "Synthesis of graphene decorated with silver nanoparticles by simultaneous reduction of graphene oxide and silver ions with glucose," *Carbon N. Y.*, vol. 59, pp. 93–99, Aug. 2013, doi: 10.1016/j.carbon.2013.02.058.

[34] M. H. Mahnashi, A. M. Mahmoud, S. A. Alkahtani, and M. M. El-Wekil, "Ivermectin detection using Ag@ B, S co-doped reduced graphene oxide nanohybrid," *J. Alloys Compd.*, vol. 871, pp. 1–8, Aug. 2021, doi: 10.1016/j.jallcom.2021.159627.

[35] T. Vi *et al.*, "The Preparation of Graphene Oxide-Silver Nanocomposites: The Effect of Silver Loads on Gram-Positive and Gram-Negative Antibacterial Activities," *Nanomaterials*, vol. 8, no. 3, pp. 1–15, Mar. 2018, doi: 10.3390/nano8030163.

[36] S. Gurunathan *et al.*, "Reduced graphene oxide-silver nanoparticle nanocomposite: A potential anticancer nanotherapy," *Int. J. Nanomedicine*, vol. 10, pp. 6257–6276, 2015, doi: 10.2147/IJN.S92449.

[37] H. Ahmad, H. S. Albaqawi, N. Yusoff, S. A. Reduan, and C. W. Yi, "Reduced Graphene Oxide-Silver Nanoparticles for Optical Pulse Generation in Ytterbium- and Erbium-Doped Fiber Lasers," *Sci. Rep.*, vol. 10, no. 1, pp. 1–11, 2020, doi: 10.1038/s41598-020-66253-w.

[38] M. S. León, R. Irizarry, and M. E. Castro-Rosario, "Nucleation and Growth of Silver Sulfide Nanoparticles," *J. Phys. Chem. C*, vol. 114, no. 13, pp. 5839–5849, Apr. 2010, doi: 10.1021/jp911238a.

[39] A. K. Suresh *et al.*, "Monodispersed biocompatible silver sulfide nanoparticles: Facile extracellular biosynthesis using the γ-proteobacterium, *Shewanella oneidensis*," *Acta Biomater.*, vol. 7, no. 12, pp. 4253–4258, Dec. 2011, doi: 10.1016/j.actbio.2011.07.007.

[40] F. ullah Khan, S. Mahmood, Z. Ahmad, T. Mahmood, and Z. A. Nizami, "Graphene oxide synthesis by facile method and its characterization," *Open J. Chem.*, vol. 2, no. 1, pp. 11–15, 2019, doi: 10.30538/psrp-ojc2019.0008.

[41] D. Khalili, "Graphene oxide: a promising carbocatalyst for the regioselective thiocyanation of aromatic amines, phenols, anisols and enolizable ketones by hydrogen peroxide/KSCN in water Department of Chemistry, College of Sciences, Shiraz University, Shiraz 7," *New J. Chem.*, vol. 40, no. 3, pp. 2547–2553, 2016.

[42] Q. Zhao *et al.*, "Synergistically improved electrochemical performance and its practical application of graphene oxide stabilized nano Ag2S by one-pot homogeneous precipitation," *Appl. Surf. Sci.*, vol. 501, pp. 1–8, Jan. 2020, doi: 10.1016/j.apsusc.2019.144208.

[43] A. Molla, Y. Li, B. Mandal, S. G. Kang, S. H. Hur, and J. S. Chung, "Selective adsorption of organic dyes on graphene oxide: Theoretical and experimental analysis," *Appl. Surf. Sci.*, vol. 464, pp. 170–177, Jan. 2019, doi: 10.1016/j.apsusc.2018.09.056.